Journal of Power Sources 299 (2015) 398–402

Contents lists available at ScienceDirect

Journal of Power Sources

journal homepage: www.elsevier.com/locate/jpowsour

Short communication

Fe-doped SnO_2 nanoparticles as new high capacity anode material for secondary lithium-ion batteries

Franziska Mueller [a, b, c], Dominic Bresser [a, c, 1], Venkata Sai Kiran Chakravadhanula [d, e], Stefano Passerini [a, c, *]

[a] Helmholtz Institute Ulm (HIU) Electrochemistry I, Helmholtzstr. 11, 89081, Ulm, Germany
[b] Institute of Physical Chemistry, University of Muenster, Corrensstr. 28/30, 48149, Muenster, Germany
[c] Karlsruher Institute of Technology (KIT), PO Box 3640, 76021 Karlsruhe, Germany
[d] Helmholtz Institute Ulm (HIU) Methods TEM, Helmholtzstraße 11, 89081, Ulm, Germany
[e] Karlsruher Institute of Technology (KIT), Institute of Nanotechnology, PO Box 3640, 76021, Karlsruhe, Germany

HIGHLIGHTS

- Nanoparticulate Fe-doped SnO_2 is reported for the first time as new lithium-ion anode material.
- Carbon-coated Fe-doped SnO_2 exhibits superior specific capacity and enhanced coulombic efficiency compared to pure SnO_2.
- Fe-doping leads to an enhanced reversibility of the Li_2O formation.
- Capacity-limited galvanostatic (de-) lithiation results in a further stabilized cycling performance.

GRAPHICAL ABSTRACT

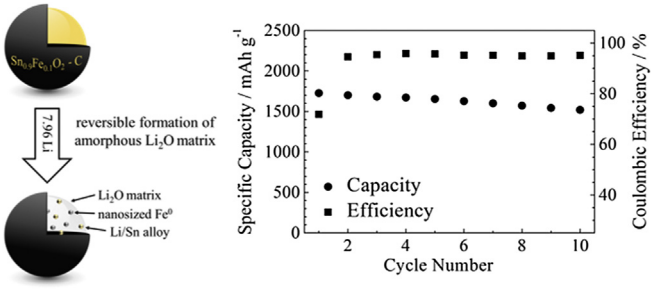

ARTICLE INFO

Article history:
Received 24 June 2015
Received in revised form
4 August 2015
Accepted 5 August 2015
Available online 16 September 2015

Keywords:
Tin oxide
Iron doping
Carbon coating
Anode
Lithium-ion battery

ABSTRACT

Herein, Fe-doped tin oxide is presented for the first time as new high-capacity lithium-ion anode material. Pure SnO_2, Fe-doped SnO_2 ($Sn_{0.9}Fe_{0.1}O_2$, SFO), and carbon-coated SFO (SFO-C) were synthesized and morphologically and electrochemically characterized by X-ray diffraction, transmission electron microscopy, thermogravimetric analysis, Brunauer–Emmet–Teller method, and galvanostatic (dis-) charge measurements. Doping SnO_2 with Fe results in a substantially enhanced reversible specific capacity and coulombic efficiency. After ten cycles the reversible capacity of SFO-C was about 1519 mAh g^{-1}, i.e., almost twice the specific capacity obtained for pure SnO_2 (764 mAh g^{-1}). Moreover, limiting the reversible capacity to 600 mAh g^{-1} shows the great potential of SFO-C for application in lithium-ion batteries.

1. Introduction

In our continuous efforts to develop high capacity, conversion-alloying anode materials for lithium-ion batteries (LIBs) [1–5], ideally characterized by low (de-)lithiation potential, high coulombic efficiency and long-term cycling stability, we

* Corresponding author.
E-mail address: stefano.passerini@kit.edu (S. Passerini).
[1] Current address: INAC/SPRAM/PCI, CEA Grenoble, UMR-5819, CEA-CNRS-UJF, 17 Rue de Martyrs, 38054, Grenoble, Cedex 9, France.

http://dx.doi.org/10.1016/j.jpowsour.2015.08.018

synthesized and investigated a new active material, Fe-doped SnO_2 ($Sn_{0.9}Fe_{0.1}O_2$, SFO). To the best of our knowledge, this is the first report on iron-doped tin oxide as active material for LIBs. Indeed, metal-doped tin oxides comprising, e.g., vanadium, manganese, iron, cobalt, or copper as dopant, were already reported in literature. Nevertheless, these studies basically focused on the investigation of their physical characteristics such as (ferro-)magnetic, optical, or structural properties [6,7]. Besides, the application of metal-doped tin oxide as gas sensors for nitric oxide and carbon dioxide and as (electrochromic) smart glasses, was investigated [8,9]. For battery applications, however, only one manuscript dealing with the utilization of molybdenum-doped SnO_2 as active material for LIBs was reported in 1999 [10], i.e., prior to the first report on transition metal oxides as conversion materials by Poizot et al. in 2000 [11]. Compared to pure tin oxide, Mo-doped SnO_2 showed a lower first cycle reversible capacity, but improved capacity retention when cycled in a rather narrow voltage range (0.0 V–1.0 V), which the authors assigned to a decreased crystallite growth upon synthesis and a favored dispersion of the electrochemically active metallic Sn, formed upon the first lithiation, due to the presence of Mo.

Within this study, pure SnO_2, SFO, and SFO-C nanoparticles were synthesized and characterized by means of X-ray diffraction (XRD), transmission electron microscopy (TEM), thermogravimetric analysis (TGA), Brunauer–Emmet–Teller (BET) method, and galvanostatic (dis-)charge measurements, *inter alia* applying an extended voltage range (0.01 V–3.0 V). It is shown that doping SnO_2 with Fe leads to a significantly enhanced specific capacity, cycling stability, and coulombic efficiency. After ten cycles SFO-C exhibits a reversible specific capacity of 1519 mAh g^{-1}, which is about twice that of pure SnO_2. These results clearly indicate that the presence of the dopant (Fe) favors the reversible formation of lithium oxide, thus, enabling the beneficial combination of lithium storage by alloying and conversion, as already reported by us with Fe-doped zinc oxide [3]. Cycling the material in the narrow potential range between 0.01 V and 1.1 V results, moreover, in a delivered capacity of 600 mAh g^{-1} of composite electrode, i.e., including the weight of the oxide and the carbon coating. This value is slightly higher than that obtainable by the alloying process of Sn present in the material. More important, however, the combined effect of the hierarchical carbon-coating and iron, the latter enabling the conversion mechanism, allow the outstanding performance of the nanostructured material for use as LIB anodes.

2. Experimental

2.1. Synthesis

SFO ($Sn_{0.9}Fe_{0.1}O_2$) was synthesized by dissolving 0.001 mol of iron gluconate dihydrate (Aldrich Chemistry) and 0.03 mol of sucrose (Fluka) in 100 mL ultrapure water. Subsequently, 20 mL acetic acid and 0.009 mol of tin acetate (Aldrich Chemistry) were gradually added. The solution was stirred for 15 min before the water was evaporated at a temperature of 180 °C. In order to dry the syrup-like solution completely, the temperature was increased to 300 °C. The obtained solid powder was calcined under ambient atmosphere for 3 h at 450 °C with an increment of 3 °C min^{-1}. The undoped tin dioxide (SnO_2) was prepared analogously without adding the iron precursor.

2.2. Carbon coating

Carbon-coated $Sn_{0.9}Fe_{0.1}O_2$ was obtained by dispersing $Sn_{0.9}Fe_{0.1}O_2$ in ultrapure water containing an equivalent weight of sucrose. The dispersion was homogenized by means of a planetary ball mill (Vario-Planetary Mill Pulverisette 4, FRITSCH, milling conditions: 2 × 45 min at 400/−800 rpm with 10 min rest in-between). After drying the mixture at 70 °C under air, the resulting powder was ground and annealed in a tubular furnace (R50/250/12, Nabertherm) under inert Ar atmosphere at 500 °C for 4 h, applying a heating rate of 3 °C min^{-1}.

2.3. Characterization

TGA of the composite material was conducted under O_2 atmosphere using a TA Instruments Q 5000. XRD analysis was performed by means of a Bruker D8 Advance equipped with a Cu X-ray tube (Cu-$K_{\alpha 1}$ radiation, λ = 154.06 pm). The specific surface area was measured by nitrogen adsorption and calculated according to the BET theory (Micrometrics ASAP 2020). TEM was performed using an aberration corrected FEI Titan 80–300 equipped with a Gatan imaging filter (Tridiem 863). For these measurements, the powder samples were dispersed onto holey carbon Au grids (Quantifoil GmbH).

2.4. Electrode preparation

For the electrode preparation the binder (sodium carboxymethylcellulose, CMC, Dow Wolff Cellulosics) was dissolved in ultrapure water and subsequently the active material as well as the conductive carbon black (Super C65®, IMERYS Graphite and Carbon) were added. The weight ratio of the active material, conductive agent, and binder was 75:20:5. After homogenizing the dispersion by ball milling, the obtained slurry was immediately cast on dendritic copper foil (Schlenk, 99.9%) with a wet film thickness of 120 μm. The coated electrode was dried and subsequently punched to disc electrodes (ø = 12 mm). Finally, the electrodes were further dried under vacuum at 120 °C for 24 h. The active material mass loading of the electrodes ranged between 1.4 and 1.8 mg cm^{-2}.

2.5. Electrochemical characterization

The electrochemical characterization was conducted in three-electrode Swagelok® cells using lithium foil (battery grade, Rockwood Lithium) as counter and reference electrodes. All cells were assembled in a glove box (MBraun UNIlab; H_2O content < 0.1 ppm, O_2 content < 0.1 ppm) under argon atmosphere. As separator FS 2226 and as electrolyte 1 M $LiPF_6$ in a 3:7 volume mixture of ethylene carbonate and diethyl carbonate (UBE) were used. Galvanostatic cycling was carried out by means of a Maccor Battery Tester 4300 at 20 ± 1 °C.

3. Results and discussion

Fig. 1 presents the XRD patterns of undoped SnO_2, SFO, and SFO-C. All samples reveal a tetragonal cassiterite structure with $P4_2/mnm$ space group (JCPDS card No. 01-070-6153). No additional reflections are observed, indicating that the materials are phase-pure, and the iron ions are successfully introduced into the tin oxide lattice.

The TEM micrograph of pure SnO_2 (Fig. 2a) shows roughly spherical particles with an average diameter of about 15 nm. The particle size is substantially decreased in SFO and SFO-C, i.e., when part of the tin is substituted by iron, to around 7–8 nm (Fig. 2b). This effect was already reported in literature for Pd-doped SnO_2 [12] and Fe- or Co-doped ZnO [3,13] and is commonly attributed to a reduced surface energy and, hence, a decreased particle growth upon the applied thermal treatment. Indeed, this finding further indicates the successful replacement

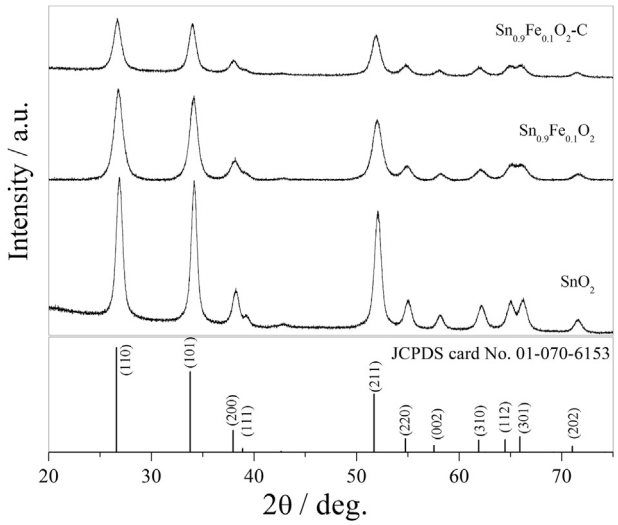

Fig. 1. XRD patterns of as-synthesized, pure SnO_2, Fe-doped SnO_2 (SFO), and carbon-coated Fe-doped SnO_2 (SFO-C); as reference given in the bottom: JCPDS card No. 01-070-6153.

of tin by iron within the cassiterite structure. In Fig. 2 (c and d) the TEM micrographs of SFO-C are presented. It is obvious, that the applied carbonaceous coating, involving an additional thermal treatment, do not have a significant impact on the particle size. Indeed, most of the particles are surrounded by a thin carbon layer (Fig. 2c, black arrow), although there are also few particles for which no carbonaceous surface layer can be detected (Fig. 2c and d, white arrow). Apart from this, however, the introduced carbon forms an electronically conductive matrix embedding and interconnecting the single nanoparticles, thus, leading to the formation of a secondary, microstructured particle morphology. The carbon content in SFO-C was determined by means of TGA, which revealed an overall carbon content of 21 wt.% with respect to the total mass of the composite. Due to the presence of the highly porous carbon, the BET surface area was as high as 94 $m^2\ g^{-1}$ compared to 63 $m^2\ g^{-1}$ for non-coated SFO and 30 $m^2\ g^{-1}$ for pure SnO_2.

Following our previous results obtained for iron-doped zinc oxide [3] and spinel-structured zinc ferrite [1,2], we focused the electrochemical characterization on pure SnO_2 and carbon-coated SFO. A comparison of the first cycle potential profiles of electrodes based on pure SnO_2 and SFO-C is presented in Fig. 3a. In case of SFO-C, the specific capacity was calculated based on the mass of the pure active material – excluding the carbon coating – to allow a direct comparison of the two active materials. For both electrodes, the potential rapidly drops to 1.5 V during the first discharge (lithiation), followed by a weakly defined feature at a potential of 1.2 V–1.3 V (A) and a more pronounced plateau at about 0.95 V (B).

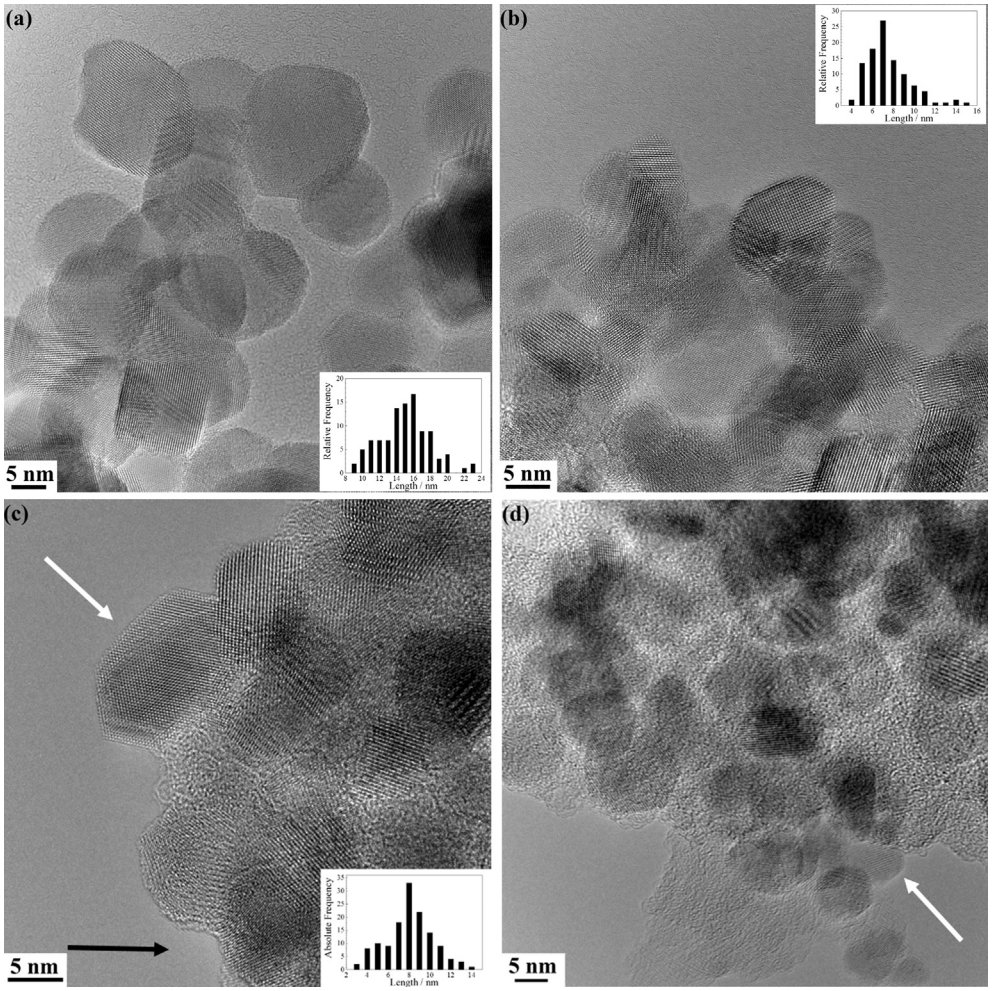

Fig. 2. TEM micrographs of as-synthesized (a) pure SnO_2 at a magnification of 300 kx (b) Fe-doped SnO_2 (SFO) at a magnification of 380 kx and (c) & (d) carbon-coated Fe-doped SnO_2 (SFO-C) at a magnification of 300 kx; accelerating voltage: 490 kV.

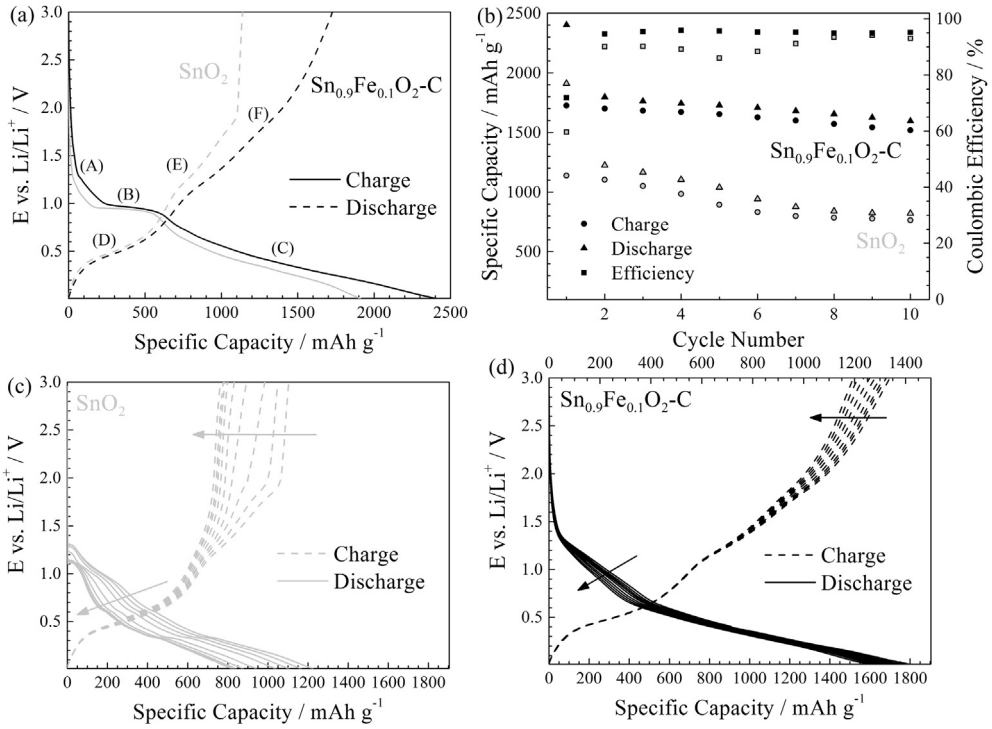

Fig. 3. Galvanostatic investigation of pure SnO_2- and SFO-C-based electrodes: (a) comparison of the 1st cycle potential profiles; (b) specific capacity *vs.* cycle number; (c) and (d) the potential profiles for the following (dis-)charge cycles for SnO_2 and $Sn_{0.9}Fe_{0.1}O_2$-C, respectively (the upper x axis in panel (d) shows the specific capacity including the mass of the carbonaceous coating); specific current: 50 mA g^{-1}, cut-off potentials: 0.01 V and 3.0 V *vs.* Li/Li^+; gray: SnO_2, black: SFO-C.

Subsequently, both samples show gently sloping potential profiles (C). The potential profile of SnO_2 is in good agreement with previously reported results for SnO_2 [11,14]. Feature (A) is assigned to the initial electrolyte decomposition and the associated solid electrolyte interphase (SEI) formation, while feature (B) is related to the reduction of tin oxide accompanied by the formation of Li_2O [14,15]. It may be noted that feature (A) is slightly more pronounced in case of SFO-C, i.e., the electrode shows a higher specific capacity in this potential range, which is presumably related to an increased electrolyte decomposition and SEI formation due to the higher specific surface area (94 m^2 g^{-1} *vs.* 30 m^2 g^{-1}). Additionally, our recent studies on transition metal-doped zinc oxide revealed that Fe^{3+} may be initially reduced to Fe^{2+} prior to the reduction of the oxide [13], which would explain a capacity gain of about 18.6 mAh g^{-1} at such potentials. The substitution of Sn^{4+} by Fe^{3+} in the cassiterite lattice, moreover, results in the formation of oxygen vacancies [13] (to compensate the charge imbalance), i.e., the formation of relatively less Li_2O upon lithiation. This effect may also explain the slightly shorter voltage plateau at about 0.95 V (B) for SFO-C compared to SnO_2. In fact, such a relative capacity increase at higher potentials (A) and capacity decrease upon the voltage plateau (B) are in very good agreement with the experimentally obtained capacity values. The following rather sloped potential profile for potentials below 1 V (C) is assigned to the alloying process of tin and lithium [14–16].

The subsequent charge (delithiation) profile exhibits three characteristic features for both active materials: (D), a plateau-like profile at rather low potentials of about 0.4 V–0.5 V, related to the dealloying process [14–16], (E), a region within which the potential increases more rapidly, attributed to the (partially) reversible decomposition of Li_2O [17], and (F), a steeper potential increase, presumably also related to the degradation of Li_2O. These last two steps lead to the reversible formation of tin and iron oxides. The comparison of region (F) for both electrodes reveals that the SnO_2-based electrode does not deliver any capacity in this high potential region, while the SFO-C-based electrode provides a reversible capacity of about 300 mAh g^{-1}.

Overall, the SnO_2- and SFO-C-based electrodes deliver a reversible capacity of 1139 mAh g^{-1} and 1726 mAh g^{-1}, respectively. It may be noted that the latter value corresponds to around 1360 mAh g^{-1}, including the mass of the carbonaceous coating, i.e., considering the total mass of the composite. Besides, the irreversible capacity loss in the first cycle is 40.4% for SnO_2 and 28.1% for SFO-C, which is obviously related to the enhanced reversible formation of Li_2O for SFO-C, due to the presence of the transition metal dopant [10,18].

Based on these results and considerations and with respect to our previously reported results for transition metal-doped zinc oxide [3], we, thus, propose the following reaction mechanism for SFO:

$$Sn_{0.9}Fe_{0.1}O_2 + 4\ Li^+ + 4\ e^- \rightarrow 2\ Li_2O + 0.1\ Fe^0 + 0.9\ Sn \quad (1)$$

$$0.9\ Sn + 3.96\ Li^+ + 3.96\ e^- \rightarrow 0.9\ Li_{4.4}Sn \quad (2)$$

Accordingly, the theoretical capacity is calculated to be 1477 mAh g^{-1}.

To evaluate the cycling stability of pure SnO_2 and carbon-coated SFO, electrodes based on these materials were subjected to continuous galvanostatic (dis-)charge tests, applying a specific current of 50 mA g^{-1} in a potential range of 0.01 V–3.0 V. The results are presented in Fig. 3b. In addition to the higher specific capacity, SFO-C exhibits an improved coulombic efficiency and stabilized capacity retention when compared to pure SnO_2. After ten cycles, SnO_2 and SFO-C provide a reversible specific capacity of 764 mAh g^{-1} and 1519 mAh g^{-1} (more precisely, 1195 mAh g^{-1} considering the contribution of carbonaceous coating), respectively. To the best of our knowledge the capacity values as obtained

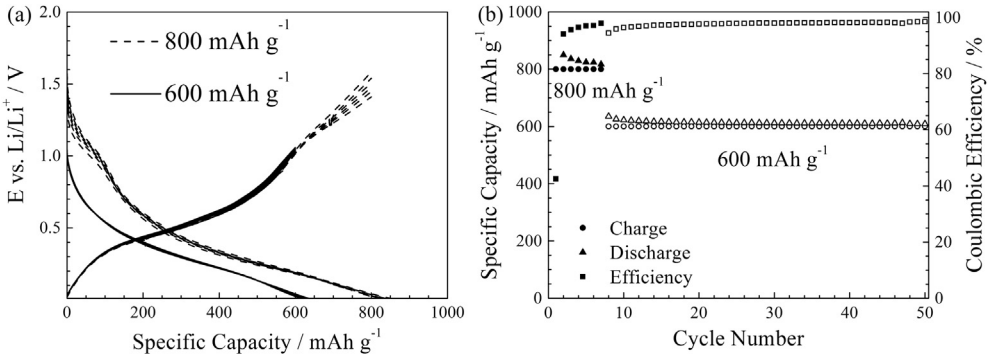

Fig. 4. Capacity-limited galvanostatic cycling of carbon-coated SFO-C-based electrodes: (a) potential profiles of the 2nd-20th cycle and (b) specific capacity *vs*. cycle number; specific current: 50 mA g^{-1}, discharge cut-off potential: 0.01 V, the capacity was limited initially to 800 mAh g^{-1} (dashed line, solid symbols) and subsequently to 600 mAh g^{-1} (solid line, open symbols).

for SFO-C, have not been reported yet for any tin-based lithium-ion anode material [14,19–24]. In addition, the coulombic efficiency exceeds all the values reported in literature for tin oxides and tin oxide/carbon composites [14,19,20,23,24].

A detailed examination of the SnO_2 electrode potential profiles clearly reveals that the substantial capacity loss upon cycling is basically related to a decreasing reversible capacity obtained at higher potentials (Fig. 3c), i.e., a decreasing reversibility of the Li_2O formation [25]. Contrarily, the evolution of the corresponding potential profiles for SFO-C shows a substantially enhanced capacity delivery at higher potentials (Fig. 3d), indicating the improved reversibility of the lithium oxide formation [3,17], which results in the increased achievable capacity and, hence, also the enhanced (1st cycle) coulombic efficiency.

In order to evaluate the practical applicability of SFO-C in a full-cell setup and having in mind that the cathode is limiting the overall full-cell capacity, (dis-)charge tests were performed within a limited capacity range. The potential profiles (Fig. 4a) and the 'specific capacity *vs*. cycle number' plot (Fig. 4b) indicate a highly stable cycling performance and a low average (dis-)charge potential, particularly when the capacity is restricted to 600 mAh g^{-1} of composite (in this test the capacity is calculated based on the total weight of the SFO-C composite). This exceptional result (more than 60% higher than that of conventional graphite) is even more interesting considering that the overall Sn content in the composite material (SFO-C) is only 58.4%. Actually, the delivered capacity in such a narrow potential range is slightly higher than that given by the alloying process of Sn (580 mAh g^{-1} of composite). More important, however, is the outstanding performance of the material in terms of coulombic reversibility and cycling stability, which is not observed in pure Sn-based electrodes.

4. Conclusions

Pure tin oxide and carbon-coated Fe-doped tin oxide nanoparticles were successfully synthesized and characterized by means of XRD, TEM, TGA, BET method, and galvanostatic cycling. Compared to pure SnO_2, SFO-C shows an improved coulombic efficiency and almost twice the specific capacity after ten cycles. Based on the herein obtained as well as previous results obtained for similar mixed conversion and alloying materials a lithium storage mechanism is proposed. Further studies are going on in our lab to evaluate the very long-term cycling stability and to consolidate the underlying reaction mechanism. Nevertheless, the superior specific capacity, rather low (de-)lithiation potential, enhanced coulombic efficiency, and improved cycling stability, certainly render iron-doped tin oxide as very promising, new, high-energy lithium-ion anode material.

Acknowledgments

Financial support from the BMW AG within the ABILE project is gratefully acknowledged. Furthermore, the authors want to thank the Karlsruhe Nano Micro Facility, a Helmholtz Research Infrastructure at KIT.

References

[1] D. Bresser, E. Paillard, R. Kloepsch, S. Krueger, M. Fiedler, R. Schmitz, D. Baither, M. Winter, S. Passerini, Adv. Energy Mater. 3 (2013) 513–523.
[2] F. Mueller, D. Bresser, E. Paillard, M. Winter, S. Passerini, J. Power Sources 236 (2013) 87–94.
[3] D. Bresser, F. Mueller, M. Fiedler, S. Krueger, R. Kloepsch, D. Baither, M. Winter, E. Paillard, S. Passerini, Chem. Mater. 25 (2013) 4977–4985.
[4] A. Varzi, D. Bresser, J. von Zamory, F. Müller, S. Passerini, Adv. Energy Mater. 4 (2014) 1400054.
[5] F. Mueller, D. Bresser, N. Minderjahn, J. Kalhoff, S. Menne, S. Krueger, M. Winter, S. Passerini, Dalton Trans. 43 (2014) 15013–15021.
[6] X.L. Wang, Z.X. Dai, Z. Zeng, J. Phys. Condens. Matter. 20 (2008) 045214.
[7] A. Bouaine, N. Brihi, G. Schmerber, C. Ulhaq-Bouillet, S. Colis, A. Dinia, J. Phys. Chem. C 111 (2007) 2924–2928.
[8] G. Zhang, M.L. Liu, Sens. Actuator B Chem. 69 (2000) 144–152.
[9] U.O. Krasovec, B. Orel, S. Hocevar, I. Musevic, J. Electrochem. Soc. 144 (1997) 3398–3409.
[10] J. Morales, L. Sanchez, J. Electrochem. Soc. 146 (1999) 1640–1642.
[11] P. Poizot, S. Laruelle, S. Grugeon, L. Dupont, J.M. Tarascon, Nature 407 (2000) 496–499.
[12] M.V. Vaishampayan, R.G. Deshmukh, I.S. Mulla, Sens. Actuator B Chem. 131 (2008) 665–672.
[13] G. Giuli, A. Trapananti, F. Mueller, D. Bresser, F. d' Acapito, S. Passerini, submitted for publication.
[14] I.A. Courtney, J.R. Dahn, J. Electrochem. Soc. 144 (1997) 2045–2052.
[15] R. Demir-Cakan, Y.S. Hu, M. Antonietti, J. Maier, M.M. Titirici, Chem. Mater. 20 (2008) 1227–1229.
[16] D. Bresser, F. Mueller, D. Buchholz, E. Paillard, S. Passerini, Electrochim. Acta 128 (2014) 163–171.
[17] X.W. Guo, X.P. Fang, Y. Sun, L.Y. Shen, Z.X. Wang, L.Q. Chen, J. Power Sources 226 (2013) 75–81.
[18] F. Wang, R. Robert, N.A. Chernova, N. Pereira, F. Omenya, F. Badway, X. Hua, M. Ruotolo, R.G. Zhang, L.J. Wu, V. Volkov, D. Su, B. Key, M.S. Whittingharn, C.P. Grey, G.G. Amatucci, Y.M. Zhu, J. Graetz, J. Am. Chem. Soc. 133 (2011) 18828–18836.
[19] I.A. Courtney, J.R. Dahn, J. Electrochem. Soc. 144 (1997) 2943–2948.
[20] X.M. Yin, C.C. Li, M. Zhang, Q.Y. Hao, S. Liu, L.B. Chen, T.H. Wang, J. Phys. Chem. C 114 (2010) 8084–8088.
[21] H.J. Ahn, H.C. Choi, K.W. Park, S.B. Kim, Y.E. Sung, J. Phys. Chem. B 108 (2004) 9815–9820.
[22] X.F. Li, A. Dhanabalan, L. Gu, C.L. Wang, Adv. Energy Mater. 2 (2012) 238–244.
[23] X.S. Zhou, Z.H. Dai, S.H. Liu, J.C. Bao, Y.G. Guo, Adv. Mater. 26 (2014) 3943–3949.
[24] J.L. Cheng, H.L. Xin, H.M. Zheng, B. Wang, J. Power Sources 232 (2013) 152–158.
[25] R. Kohler, H. Besser, M. Hagen, J. Ye, C. Ziebert, S. Ulrich, J. Proell, W. Pfleging, Microsyst. Technol. 17 (2011) 225–232.